

Article

Selecting Appropriate Spatial Scale for Mapping Plastic-Mulched Farmland with Satellite Remote Sensing Imagery

Hasituya, Zhongxin Chen *, Limin Wang and Jia Liu

Key Laboratory of Agricultural Remote Sensing, Ministry of Agriculture, P.R. China (AGRIRS)/Institute of Agricultural Resources and Regional Planning, Chinese Academy of Agricultural Sciences, No. 12, Zhongguancun Nan Dajie, Haidian District, Beijing 100081, China; 2009hasituya@sina.com (H.); wanglimin01@caas.cn (L.W.); liujia_hh@126.com (J.L.)

* Correspondence: chenzhongxin@caas.cn; Tel.: +86-10-8210-5089

Academic Editors: Jan Dempewolf, Jyoteshwar Nagol, Min Feng, James Campbell and Prasad S. Thenkabail
Received: 30 November 2016; Accepted: 12 March 2017; Published: 14 March 2017

Abstract: In recent years, the area of plastic-mulched farmland (PMF) has undergone rapid growth and raised remarkable environmental problems. Therefore, mapping the PMF plays a crucial role in agricultural production, environmental protection and resource management. However, appropriate data selection criteria are currently lacking. Thus, this study was carried out in two main plastic-mulching practice regions, Jizhou and Guyuan, to look for an appropriate spatial scale for mapping PMF with remote sensing. The average local variance (ALV) function was used to obtain the appropriate spatial scale for mapping PMF based on the GaoFen-1 (GF-1) satellite imagery. Afterwards, in order to validate the effectiveness of the selected method and to interpret the relationship between the appropriate spatial scale derived from the ALV and the spatial scale with the highest classification accuracy, we classified the imagery with varying spatial resolution by the Support Vector Machine (SVM) algorithm using the spectral features, textural features and the combined spectral and textural features respectively. The results indicated that the appropriate spatial scales from the ALV lie between 8 m and 20 m for mapping the PMF both in Jizhou and Guyuan. However, there is a proportional relation: the spatial scale with the highest classification accuracy is at the 1/2 location of the appropriate spatial scale generated from the ALV in Jizhou and at the 2/3 location of the appropriate spatial scale generated from the ALV in Guyuan. Therefore, the ALV method for quantitatively selecting the appropriate spatial scale for mapping PMF with remote sensing imagery has theoretical and practical significance.

Keywords: plastic-mulched farmland (PMF); mapping; appropriate spatial scale; GF-1 satellite imagery; local variance function; supervised classifier

1. Introduction

The plastic mulching technique has been applied extensively both in China and in the rest of the world, due to its positive effects of improving hydrothermal conditions in farmland, promoting crop growth, expanding planting area and increasing crop yield. Plastic film is widely used for covering greenhouses, medium or low tunnels and for mulching. China has the largest area of plastic-mulched farmland (PMF) in the world, and that area has been growing more and more rapidly. The 0.12 million ha area mulched by plastic film in 1981 increased to 19.79 million ha in 2011 [1] and to 25 million ha in 2013 [2]. From the view of the short-term agricultural production, the practices of plastic mulching bring many benefits to farmers by avoiding unfavorable growing conditions. However, due to the special properties of plastic film itself and its expansive and unreasonable use, a set of environmental

problems have been raised and have become more and more serious. For example, the accumulated plastic residues over years have caused deterioration of the soil structure, farmland quality degradation, crop yield reduction and environmental pollution. Furthermore, plastic mulching may result in the imbalance of energy and matter cycling. Such phenomena have been becoming more and more serious in recent years [1,3]. Considering both the agricultural production and environmental protection and both to the long-term and immediate interests, a full spatial and temporal picture of PMF is demanded for many applications, decision-making and research departments. This is also essential for updating the land cover database and the development of local policies. However, the field survey is time-consuming, cost-expensive and labor-exhausting over large regions and a long time. Remote sensing is recognized as a plausible tool and cost-effective technique which is effective and reliable in ground objects detection. Up to now, remote sensing has been successfully used in land cover/use classification and special object mapping, including water bodies, built-up areas and crops and so on.

Nevertheless, relatively fewer researches have been conducted to map the spatial pattern, distribution area and the spatio-temporal variation of PMF with remote sensing. Wang et al. [4] discussed how to differentiate the plastic-mulched paddy field from the water background. Lu et al. [5] extracted the plastic-mulched cotton farmland from Landsat-5 TM data using a decision tree classifier. Subsequently, they [6] developed a threshold model for mapping plastic-mulched cotton fields using MODIS time series data. Hasituya et al. [7], mapping the PMF by Landsat-8 OLI imagery using the spectral and textural features, reached the conclusion that the addition of textural features from Landsat-8 OLI imagery provides only limited improvement in accuracy. From the aforementioned review, we found that (1) there was relatively less attention paid to mapping the PMF (four papers); (2) the remote sensing data for mapping PMF were medium or coarse spatial resolution imagery, the high-spatial-resolution imagery has not been used until now; (3) there were no studies with an emphasis on the selection of the appropriate spatial scale for remote mapping of PMF.

Due to the very fragmented farmland in China (including for PMF), remote mapping of PMF is hindered by its mixed spectral response because of the inadequate spatial resolution. This leads to error in area and distribution estimation. The specifications of the imagery, to a large degree, determine the accuracy of the parameter estimates [8]. Spectral resolution is especially crucial [9], but the spatial resolution may also have significant implications for remote sensing application in agriculture. Sufficient consideration of the spatial scale for mapping objects is an important facet because of the undesirable mapping accuracy from the coarser spatial resolution imagery and the difficulty and costliness of acquiring the high spatial resolution imagery over a large area and a long time. As the spatial resolution of remote sensing data is finer than the spatial size of interested objects, too much detailed or devalued information may be generated and result in larger data volume. When the spatial resolution is coarser than the spatial size of the detected objects, there exist mixed pixels which result in mismatched results. Therefore, effective methods need to be developed where each investigated object can be considered at its 'optimal' spatial scale [10], where the information, per pixel, is maximized [11]. Moreover, the spatial resolution of remote sensing imagery must be appropriate for the specific application [12] and the data should be used with caution of the potential problems caused by mismatches in scale between the sensor and the practical requirements of the mapping exercise [13]. The appropriate spatial scale for mapping is influenced by the spatial structure of the interested objects, the specifications of sensors and imagery processing designs, e.g., spectral classification, regression, texture analysis [14]. Spatial scale is one of the dominant limiting factors in minimizing within-class spectral variance and simultaneously maximizing inter-class variance. In recent years, many studies [8,14–17] have discussed the spatial scale effect of remote sensing data for object detection or parameter estimation; more studies were focused on vegetation (especially forest) and built-up area and so on; less studies put emphasis on agriculture [11]. No research effort has been made to explain the effect of spatial scale on the mapping accuracy of PMF with remote sensing until now. Therefore, it is important to evaluate the effect of spatial scale on the mapping accuracy of PMF.

This study was the first attempt to elucidate the spatial scale effect of mapping PMF using high spatial resolution imagery. More specific objectives of this work were (1) to detect the appropriate spatial scale or a range of appropriate spatial scales for mapping PMF with remote sensing; (2) to examine the spatial scale effects on the mapping accuracy of PMF by using a SVM classifier based on the spectral, textural and the combined spectral and textural features.

2. Study Area

Two study areas (Figure 1) were selected in this paper to discuss the appropriate spatial scale for mapping PMF. The one study area, Jizhou, Hebei Province in China, is a part of the North China Plain. Jizhou is situated between 37°18'40''N–37°44'25''N latitude and 115°09'57''E–115°41'07''E longitude, and occupies a 9.22×10^4 ha area, in which farmland occupies 5.93×10^4 ha [18] (approximately 64.36% of the total area). This study region has a warm temperate continental monsoon climate with a dry and windy spring, hot and rainy summer, and a cold and dry winter. The natural elements and extensive anthropogenic influences make it possible to broadly classify the land cover/use types within this area into farmland, woodland, grassland, residential land, industrial land and water body as the main land cover/use types. The major crops in this region are cotton, winter wheat and corn. Cotton fields have been widely mulched by white plastic film during the past 20 years in Jizhou.

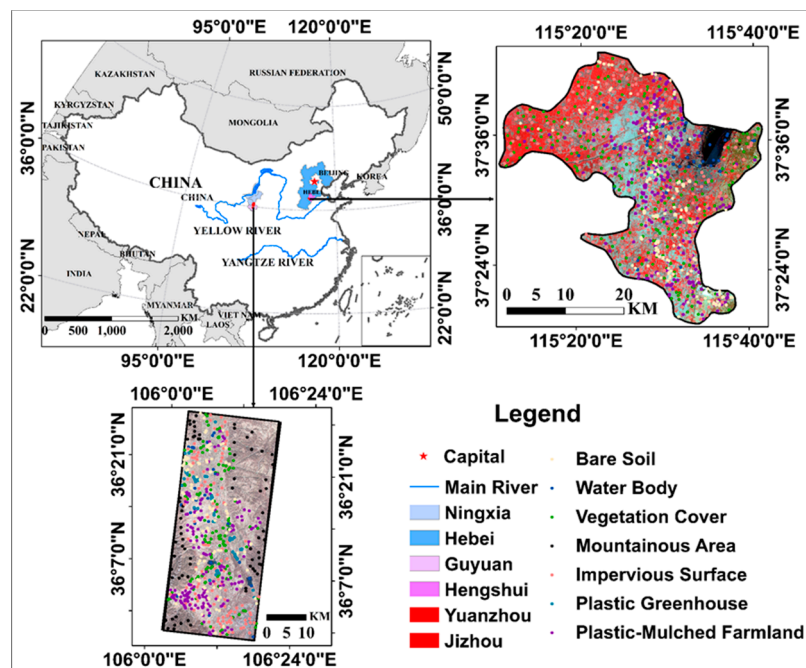


Figure 1. Location of the study area (the imagery displayed in the figure is the GaoFen-1 (GF-1) imagery in false color composite: R = Near Infrared, G = red, B = green).

Another study area is Guyuan, Ningxia Hui Autonomous Region, China. Ningxia is one of the ecological barriers of the western region of China. This area has a temperate continental semi-arid climate with warm spring, hot summer, cool autumn and cold winter, and this area is characterized by an arid climate, less rainfall, more evaporation and insufficient irrigation facility. The annual average temperature is 5.4–10.0 °C, annual precipitation is 169.5–611.8 mm, annual sunshine duration is 2800 h, and frost-free period is 148 d [19]. The total area is 5.19×10^6 hm², and the farmland area is 110.35×10^4 hm². Among the farmland, paddy field is 4.05×10^4 hm², irrigated land is 36.99×10^4 hm², garden is 3.33×10^4 hm², woodland is 60.36×10^4 hm² and grassland is 233.09×10^4 hm² [20,21]. This area is one of the typical regions of plastic-mulching with the most obvious mulching effect. The mulched crops include corn, winter wheat and some

vegetable. Mulching practice in Guyuan includes mulching in autumn, mulching in early spring and mulching before planting.

These two study areas are different in the natural condition and in the agricultural production mode, particularly, the plastic mulching practice is different in these two study areas. Therefore, these two study areas can represent the typicality of plastic mulching practices in China to some extent.

3. Data and Methods

3.1. Data and Preprocessing

3.1.1. Remote Sensing Data

The GaoFen-1 (GF-1) satellite was launched on 26 April 2013, and represents the first satellite for the civilian High-Definition Earth Observation Satellite (HDEOS) program implemented in China [22]. The GF-1 satellite carries two high spatial resolution cameras (GF1-PMS1 and GF1_PMS2) with 60 km width and four medium spatial resolution wide field-of-view cameras (WFV) with 800 km width. The GF-1/PMS have one panchromatic band with a 2 m spatial resolution and four multispectral bands with 8 m spatial resolution (Table 1), and the WFV sensors have four multispectral bands with 16 m resolutions. Because the remote sensing characteristic of PMF is influenced greatly by mulched crops and soil, as well as dust and rainfall after it has been mulched, the optimal mapping period is just after mulching. The advantages of the GF-1 satellite are the high spatial resolution that provides more detailed spatial structural information and high temporal resolution that can capture the key periods of mapping.

The cotton (the only plastic-mulched crop in Jizhou) is planted from mid-to-late April and seedlings emerge between late April and early May. The corn (the dominant plastic-mulched crop in Guyuan) is planted in early spring, and the farmland is mulched in autumn or in early spring. Thus, we selected four scenes of GF-1 PMS1 high quality imagery acquired on 5 May 2015 and two scenes of GF-1 PMS2 acquired on 11 June 2015 in Jizhou, and two scenes of GF-1 PMS1/2 cloud-free imagery acquired on 8 April 2014 in Guyuan. The GF-1 imagery, both in Jizhou and Guyuan, was radiometrically (using the calibration parameters of 2015 in Jizhou and of 2014 in Guyuan) and atmospherically calibrated using FLAASH (Fast Line of-sight Atmospheric Analysis of Spectral Hypercubes). The ortho-rectification (using the RPC file in system) and geometric rectification (using the pan band of landsat-8 OLI imagery acquired on 16 April 2015 in Jizhou and on 7 April 2014 in Guyuan) were performed as well. The imagery within study areas was obtained by mosaicking and clipping. Due to the west region of the Guyuan being a large mountainous area and there being fewer PMF, the mountainous area is masked from the region of Guyuan, therefore the east region of Guyuan and the whole region of Jizhou were obtained for the experiment.

Table 1. Parameters of GF-1 satellite data.

Sensor	Band	Wavelength	Spatial Resolution
PAN	Pan	0.45–0.90 μm	2 m
MSS1	Blue	0.45–0.52 μm	8 m
MSS2	Green	0.52–0.59 μm	8 m
MSS3	Red	0.63–0.69 μm	8 m
MSS4	Near Infrared (NIR)	0.77–0.89 μm	8 m

3.1.2. Ground Reference Data

Ground reference data were collected by field investigation and visually interpreting high spatial resolution imagery.

The initial ground reference data in Jizhou were gathered as point samples by field investigation during the period 25–30 April 2015. Then, using the collected point samples, we created the polygon

samples by visually interpreting the GF-1 satellite 2 m spatial resolution pan-sharpened imagery. The 60 m × 60 m sized ground reference data include 1135 polygon samples which were collected in Jizhou (Table 2).

The ground reference data in Guyuan were collected by visually interpreting the GF-1 satellite 2 m spatial resolution pan-sharpened imagery. In total, we collected 647 polygon samples (60 m × 60 m sized) for land cover/use types (Table 2). The samples were distributed throughout the whole region and the samples of each study area were divided into two halves for training and testing samples separately.

Table 2. The land cover classification scheme and samples in Jizhou and Guyuan.

Land Cover Types	Remarks	Jizhou	Guyuan	Final Types
Plastic-Mulched Farmland (PMF)	White Plastic Film	255	167	PMF
Impervious Surface	Buildings, Factories, Roads and Dam Boundaries	301	110	Non-PMF
Vegetation Cover	Crop, Vegetable Field, Grassland, Woodland	305	122	
Water Body	Rivers, Lakes and Irrigation Canals	74	25	
Bare Soil	Bare Land, Fallow land and Abandoned Land	200	98	
Plastic Greenhouse	Walk-in or medium plastic tunnel	-	54	
Mountainous Area	Mountainous Area	-	71	

3.2. Methods

In this paper, the ALV (Average Local Variance) method was used to investigate the appropriate spatial scale for mapping PMF in two study areas based on GF-1 data. Afterwards, in order to validate the effectiveness of the ALV method and to interpret the relationship between appropriate spatial scales obtained from the ALV and the spatial scale with the highest classification accuracy, we classify the imagery with different spatial resolution by means of SVM and assess the classification accuracy.

3.2.1. The Average Local Variance Function (ALV)

To determine an appropriate spatial scale for mapping the PMF with remote sensing, the ALV function presented by Woodcock et al. in 1987 [23] was applied in this paper. Local variance is a texture statistic that has been shown to characterize the relationship between spatial resolution and objects size [8]. The rationale of the local variance method is that if the spatial resolution of remote sensing data is finer than the size of interested objects, one object composed by several pixels and most of the neighboring pixels will be highly correlated and the local variance will be low. If the spatial resolution of remote sensing data is approximate to the size of the interested object, one object composed of almost one pixel and neighboring pixels belong to different objects, the local variance will be raised. If the spatial resolution of remote sensing data is coarser than the size of the investigated object, then one pixel contains several different objects and the local variance will be decreased [14]. The ALV obtain the mean values of the standard deviation of all pixels in all moving windows of the entire imagery, before plotting the average local variance curves against the varying spatial resolution. Furthermore, we can determine the appropriate spatial resolution for detecting a ground object in the light of a peak value of a local variance plot that is closely related to the spatial pattern of the object. Many studies applied the ALV function to determine the appropriate spatial scale for objects detection or parameter estimation. Hyppanen et al. [24] selected the optimal spatial scale of remote sensing data for detecting the autocorrelation size of coniferous forest. Coops et al. [25] applied the local variance method for detecting the space pattern of forest based on simulated high spatial resolution imagery. Song et al. [26] applied the local variance method for evaluating the spatial pattern of forest. Drăguț et al. [27] applied the local variance method to DEM data for studying the spatial changes of the surface topography parameters. The ALV is computed by four steps generally. These steps include (1) selecting the representative subset imagery that adequately characterizes the investigated object; (2) aggregating the imagery progressively to obtain a series of imagery with varying spatial resolutions; (3) calculating the ALV at each aggregated spatial resolution and (4) plotting the average

local variance plots against the varying spatial resolution for determining the appropriate spatial scale for ground objects detection.

In this paper, the GF-1 satellite panchromatic and multispectral (PMS) imagery were pan-sharpened to 2 m resolution multi-spectral imagery and the subsets in each study area were generated to represent the PMF. In each subset, the imagery was resampled from 2 m to 80 m with an increment of 2 m. The ALV was, then, calculated at each imagery with different spatial resolution at a fixed moving window.

(1) Selection of representative subsets

The objective of this step was to determine the representative subset imagery for calculating local variance. In this paper, we selected three representative PMF subsets which are predominant in the 500 m × 500 m sample plot respectively for two study areas from a 2 m pan-sharpened imagery (Figure 2).

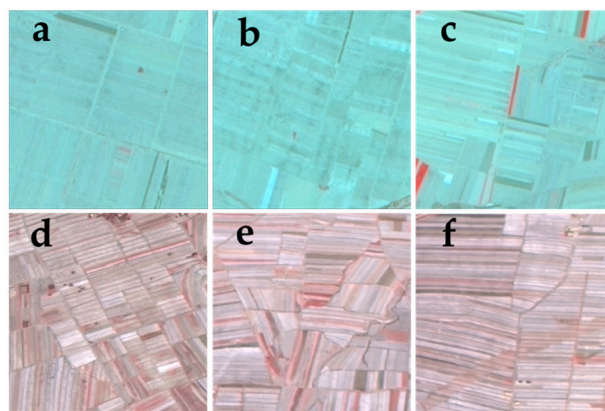


Figure 2. The PMF representative subset imagery (R = NIR, G = Red, B = Green) for determining the appropriate spatial resolution (a–c are the representative subsets in Jizhou; and d–f are the representative subsets in Guyuan).

(2) Aggregating the spatial resolution of the subset imagery

In this section, each band of 2 m pan-sharpened multi-spectral subset imagery was aggregated progressively using the nearest neighboring algorithm to obtain a series of imagery with varying spatial resolutions. Many studies [10,28,29] support the utility of the nearest neighboring approach to resample the remote sensing imagery. The aggregating way includes arithmetic progression and geometric progression. In this paper, the arithmetic progression was used to aggregate each band of 2 m pan sharpened imagery to generate the varying spatial resolution imagery from 2 m to 80 m with an increment of 2 m. We obtained 480 (40 imagery with decreasing spatial resolution × 4 bands × 3 representative samples) single-band imagery with varying spatial resolution imagery in Jizhou and Guyuan respectively.

(3) Calculating the ALV

In this section, the ALV was calculated for three representative subsets using four GF1_PMS pan sharpened bands. In this paper, in order to cover the objects with different patch sizes approximately, we designed odd sized moving window n pixels × n pixels ($n = 3, 5, 7$ and 9) to compute the ALV at each aggregated spatial resolution imagery. Equations (1) and (2) were used to compute the ALV for each representative subset [30].

$$G = \frac{\sum_{i=0}^{M-1} \sum_{j=0}^{N-1} G(i, j)}{MN} \quad (1)$$

$$s^2 = \frac{\sum_{i=0}^{M-1} \sum_{j=0}^{N-1} [G(i, j) - G]^2}{MN} \quad (2)$$

where, i and j are the row and column, $G(i, j)$ is the gray level at row i and column j , S^2 is the ALV, M and N are the row and column of the moving window.

(4) Plotting the curves of ALV against the varying spatial resolutions

The concept behind the ALV function is that a peak of maximal variance appears at a spatial resolution that is closely related to the dominant size of the interested object in the imagery [31,32]. To determine the appropriate spatial scale or a range of appropriate spatial scales for mapping PMF, the ALV curves were plotted against the decreasing spatial resolution for each representative subset and each moving window size.

3.2.2. Sharpening and Resampling

For further feature extraction and classification, the multispectral imagery with 8 m spatial resolution was pan-sharpened to obtain 2 m spatial resolution pan-sharpened multispectral imagery in the whole study area using the Gram-Schmidt pan sharpening approach. Then, the nearest neighbor resampling method was used to aggregate the 2 m spatial resolution pan-sharpened multispectral imagery to obtain a set of (2 m, 4 m, 8 m, . . . , 98 m, 100 m, 110 m, 120 m, . . . , 240 m and 250 m) varying spatial resolution imagery of the whole study area.

3.2.3. Gray Level Co-Occurrence Matrix

With the development of remote sensing technology, high spatial resolution satellite data, which provide more detailed spatial structural information, have recently become readily available. However, classifications using spectral information alone have proved to be inadequate for high spatial resolution imagery due to the mixed and complex spectral characteristics within the same land cover type and among different land cover types. The high spatial resolution imagery provides more abundant texture details and spatial structural information compared with the medium resolution imagery. The textural features have long been recognized as valuable spatial information in discriminating different land cover types with very similar spectra. Furthermore, the PMF exhibits significant textural characteristics. The PMF is distributed in a rectangular shape in a large region of our study area, so the texture regularity of PMF is significant. In order to prevent flooding when there is heavy rain, in most cases, the PMF is separated by other non-plastic-mulched crops in a certain width, thus the changing degree of gray level carries a certain regularity. The white plastic film used in these two study areas is a thin smooth film surface, therefore, it will reduce the soil surface roughness to a certain degree, thus the surface roughness/smoothness of PMF differ from other land cover types. Therefore, the textural feature of the PMF should make a great contribution for separating the PMF from the other land cover types. However, the contribution of the textural features from high spatial resolution imagery has not been explained for mapping PMF.

Many textural feature extraction methods, such as gray level co-occurrence matrix (GLCM), Markova random field, the fractal model and the wavelet transform method, have been proposed and tested. Among them, the GLCM is one of the most popular methods for texture analysis [33,34] and performs better than other methods in most cases [35–38]. The GLCM, first presented by Haralick in 1973 [39], contains the relative occurrence frequencies of the digital number of pair pixels at a relative fixed orientation and distance in imagery [40]. Eight commonly used statistical measures, such as mean, variance, homogeneity, contrast, dissimilarity, entropy, angular second moment and correlation, can be generated from the GLCM to describe the textural characteristics of objects.

The mean reflects the regularity of texture. It is smaller for indescribable desultorily textures and larger for describable regularity texture. The variance reflects the non-uniformity of texture in imagery. The contrast represents the clarity of imagery and the strength of the texture. Homogeneity

represents the smoothness of the gray level distribution of imagery. There is a negative correlation between contrast and homogeneity. Dissimilarity is a measure of the changing degree of the gray level in imagery. There are positive correlations between contrast and dissimilarity. Entropy is an index reflecting the information of the imagery. The angular second moment, also called the energy, is a measurement of the distribution uniformity of the gray level in imagery. A greater value of the angular second moment represents a coarser texture. Correlation refers to the relationship between a reference pixel and its neighbouring pixels throughout an entire imagery [41]. Each GLCM statistical measurement can be used to classify the imagery together with the spectral features.

The textural features are directly related to the computing window size, distance, orientation, and quantization level [42]. In this paper, eight commonly used textural features over all spatial resolutions imagery (2 m to 250 m) were computed with a 3 pixels \times 3 pixels window size, 1 pixel distance, 45° orientation and gray scale quantization level of 64. A mirror extension method was used to obtain the textural feature from the pixels on the border of the imagery.

3.2.4. Supervised Classification

Determination of the appropriate spatial scale or a range of appropriate spatial scales is to improve the mapping accuracy, thus enabling the effectiveness of the ALV to be evaluated by the classification accuracy. The Support Vector Machine (SVM) was applied to map the PMF in two study areas and the relationship between the appropriate spatial scale from the ALV and the spatial resolution with the highest classification accuracy was analyzed.

After extracting textural features from the varying spatial resolution imagery, we developed three feature sets for each spatial resolution: (1) the spectral features (reflectance of four bands) of imagery at varying spatial resolution (2 m to 250 m); (2) the textural features (eight textural features from each band) generated from imagery with varying spatial resolution; and (3) the combined spectral and textural features, the textural features with fixed spatial resolution stacked with spectral features (reflectance of four bands) of corresponding scale. Each newly combined spectral and textural feature set contains four spectral bands and 32 textural features obtained from imagery with a fixed spatial resolution. Thus, 65 combined spectral and textural features were formed across the spatial resolutions from 2 m to 250 m.

The SVM algorithm is a well-known classifier in the machine learning field and has been successfully used in a wide range of classification problems in remote sensing [43]. Various studies have shown that the SVM classifier outperforms other classifiers in most cases [44–48]. The concept behind SVM is based on minimizing the structural risk and maximizing the separating margin [49]. The measures of overall accuracy (OA), kappa coefficient (Kappa), producer's accuracy (PA) and user's accuracy (UA) were used to assess the performance of the supervised classifier. The OA is defined as the ratio of the total correctly classified pixels to the total number of pixels (the total number of all ground truth reference pixels). The PA corresponds to omission error and the UA corresponds to commission error.

4. Results and Discussion

4.1. Results

4.1.1. The Appropriate Spatial Resolution for Mapping the PMF

In this paper, we selected three representative samples of PMF and computed their ALVs and then obtained the local variance plots of PMF in Jizhou (Figure 3) and in Guyuan (Figure 4) at a computing window size of 3 pixels \times 3 pixels (upper left), 5 pixels \times 5 pixels (upper right), 7 pixels \times 7 pixels (lower left) and 9 pixels \times 9 pixels (lower right).

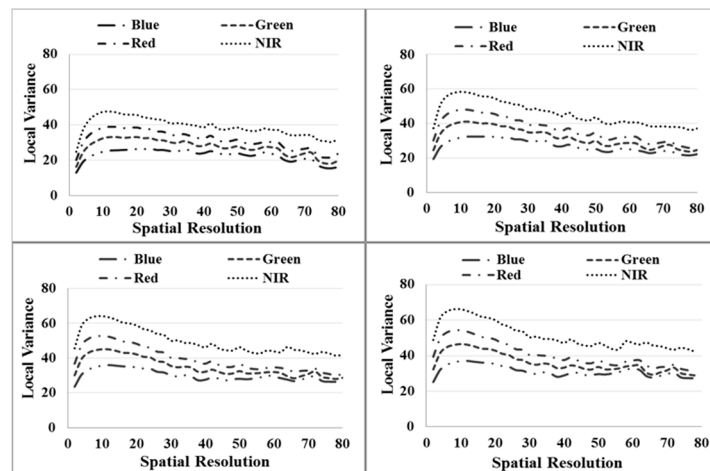


Figure 3. Local variance plots of PMF in Jizhou.

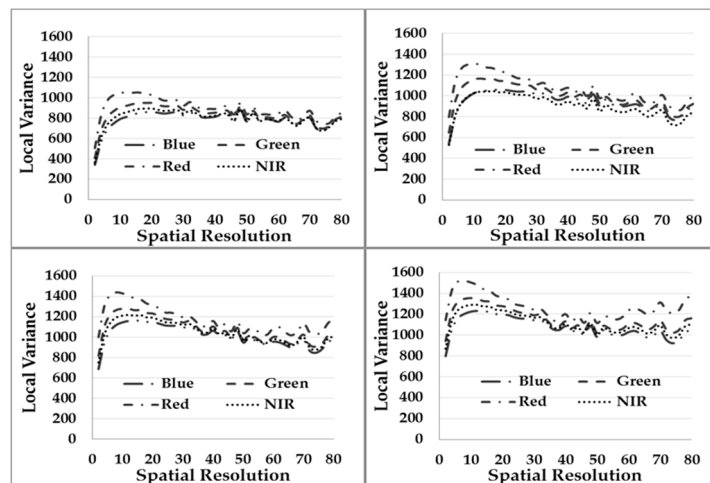


Figure 4. Local variance plots of PMF in Guyuan.

From Figures 3 and 4, we can see that each local variance plot has a peak value; this was an ideal result and agreed with the presumption of the local variance algorithms. Therefore, these were ideal results for selecting the appropriate spatial scale for mapping PMF. However, there were slight differences among the different computing window sizes. The location of the peak values in the local variance plot was moved to the left with the increasing window size and the shape of the local variance plots became more obvious.

The appropriate spatial scale obtained from the ALV for mapping the PMF in Jizhou and Guyuan is presented in Table 3. From the table, we can see that the peak value of local variance ranged between 8 m and 20 m in Jizhou and Guyuan across the different moving window sizes and different bands. There was a certain degree of difference in the peak value generated from different bands.

Table 3. The appropriate spatial scales obtained from the average local variance (ALV) in Jizhou and Guyuan.

Moving Window (Pixels)	Bands	Appropriate Spatial Resolution (m)	
		Jizhou	Guyuan
3 × 3	Blue	20	20
	Green	14	16
	Red	12	16
	NIR	12	14
5 × 5	Blue	18	16
	Green	12	12
	Red	12	10
	NIR	10	8
7 × 7	Blue	12	16
	Green	10	12
	Red	10	8
	NIR	10	8
9 × 9	Blue	10	16
	Green	10	10
	Red	8	8
	NIR	8	8

4.1.2. Classification Results

(1) Classification Accuracy and Its Variation

Figures 5 and 6 illustrate the classification accuracies generated from spectral features, textural features and the combined spectral and textural features across varying spatial resolution imagery (a part of spatial resolutions) in Jizhou and Guyuan. It can be found that differences in accuracies (including the OA, PA and UA) were observed in different feature sets and study areas.

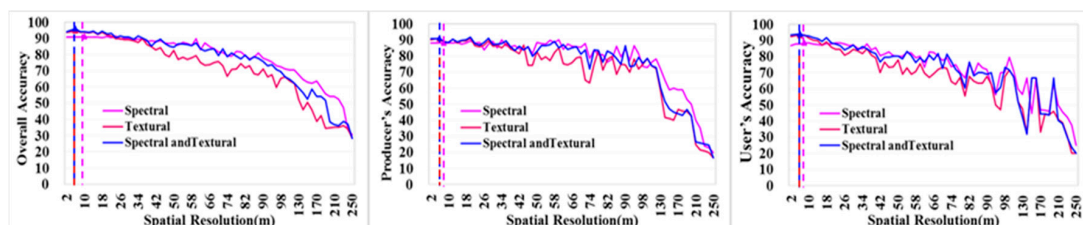


Figure 5. The variations in overall, producer's and user's accuracies of mapping PMF in Jizhou (vertical line show the highest accuracy of different features sets).

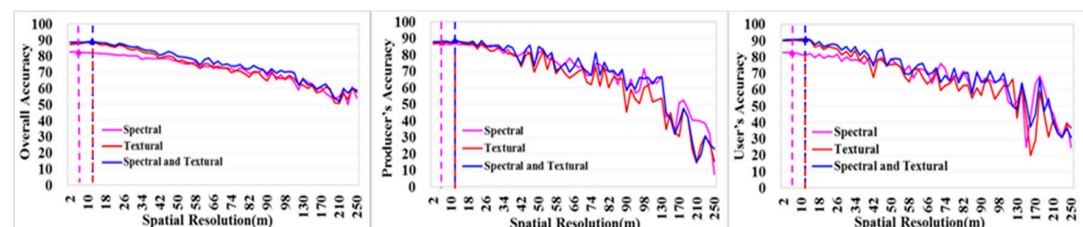


Figure 6. The variations in overall, producer's and user's accuracies of mapping PMF in Guyuan (vertical line shows the highest accuracy of different features sets).

In Jizhou, for the spectral based classification, the OA reached the highest level of 91.16% at a spatial resolution of 10 m, and the PA and UA achieved the highest value of 88.30% and 88.59% at a

spatial resolution of 8 m respectively. For the textural based classification, the OA reached the highest level of 95.95% at a spatial resolution of 6 m, and the PA and UA achieved the highest value of 90.85% and 93.58% at a spatial resolution of 6 m and 8 m respectively. For the combined spectral and textural feature based classification, the OA, PA and UA reached the highest level of 96.05%, 90.99% and 94.22% all at a spatial resolution of 6 m.

In Guyuan, for the spectral based classification, the OA, PA and UA achieved the highest value of 82.79%, 87.10% and 82.86% all at a spatial resolution of 6 m. For the textural based classification, the OA reached the highest level of 89.01% at a spatial resolution of 12 m, and the PA and UA achieved the highest value of 88.58% and 90.38% at the spatial resolution of 12 m and 8 m, respectively. For the combined spectral and textural based classification, the OA, PA and UA reached the highest level of 89.511%, 88.34% and 90.92% all at a spatial resolution of 12 m.

For the variation in OA, PA and UA for mapping PMF over varying spatial resolution imagery, we can see that when the spatial resolution changed from 2 m to 250 m, decreases were observed in OA, PA and UA as a general tendency. However, the varying trend in accuracies depends on the different feature sets and different study areas.

For Jizhou, as the spatial resolution coarsened from 2 m to 32 m, the OA, PA and UA generated from spectral features alone decreased by 1.59%, 2.95% and 1.46% respectively. The OA, PA and UA generated from textural features alone decreased by 5.27%, 3.36% and 9.01% respectively. In addition, the OA, PA and UA generated from the combined spectral and textural features decreased by 4.75%, 3.25% and 9.46% respectively. As the spatial resolution coarsened from 32 m to 100 m, the OA, PA and UA generated from spectral features alone decreased by 17.94%, 12.21% and 5.70% respectively. The OA, PA and UA generated from textural features alone decreased by 22.07%, 8.10% and 11.81% respectively. In addition, the OA, PA and UA generated from the combined spectral and textural features decreased by 23.02%, 8.10% and 12.36% respectively. As the spatial resolution coarsened from 100 m to 250 m, the OA, PA and UA generated from spectral features alone decreased by 40.57%, 52.86% and 54.59%. The OA, PA and UA generated from textural features alone decreased by 38.28%, 61.90% and 51.74%. In addition, the OA, PA and UA generated from the combined spectral and textural features decreased by 38.28%, 61.90% and 51.74% respectively. Furthermore, as the spatial resolution coarsened from 2 m to 250 m, the OA, PA and UA generated from spectral features alone decreased by 60.10%, 68.02% and 61.75% respectively. The OA, PA and UA generated from the textural features alone decreased by 65.61%, 73.36% and 72.56% respectively. In addition, the OA, PA and UA generated from the combined spectral and textural features decreased by 66.04%, 74.05% and 73.56% respectively.

For Guyuan, as the spatial resolution coarsened from 2 m to 32 m, the OA, PA and UA generated from the spectral features alone decreased by 2.34%, 1.53% and 2.58% respectively. The OA, PA and UA generated from the textural features alone decreased by 3.39%, 4.00% and 6.58% respectively. In addition, the OA, PA and UA generated from the combined spectral and textural features decreased by 2.90%, 2.09% and 4.22% respectively. As the spatial resolution coarsened from 32 m to 100 m, the OA, PA and UA generated from the spectral features alone decreased by 13.25%, 23.59% and 13.39% respectively. The OA, PA and UA generated from the textural features alone decreased by 15.94%, 20.92% and 20.78% respectively. In addition, the OA, PA and UA generated from the combined spectral and textural features decreased by 15.11%, 19.49% and 15.90% respectively. As the spatial resolution coarsened from 100 m to 250 m, the OA, PA and UA generated from the spectral features alone decreased by 12.88%, 54.07% and 41.67%. The OA, PA and UA generated from the textural features alone decreased by 10.22%, 46.38% and 26.02%. In addition, the OA, PA and UA generated from the combined spectral and textural features decreased by 11.77%, 43.10% and 39.53% respectively. As the spatial resolution coarsened from 2 m to 250 m, the OA, PA and UA generated from the spectral features alone decreased by 28.46%, 79.19% and 57.64% respectively. The OA, PA and UA generated from the textural features alone decreased by 29.55%, 71.30% and 53.38% respectively. In addition, the OA, PA and UA generated from the combined spectral and textural features decreased by 29.78%, 64.68% and 59.65% respectively.

The decrease in accuracy was larger for the textural feature alone than the spectral feature alone, from 2 m to 32 m and from 32 m to 100 m; and was larger for the spectral feature alone than the textural feature alone, from 100 m to 250 m. From 2 m to 250 m, the larger decrease in accuracy was observed for the textural feature alone. The smallest decrease in accuracy was observed at the range from 2 m to 32 m, the larger decrease was observed from 32 m to 100 m and from 100 m to 250 m, regardless of the study areas and the feature sets.

The textural features from the fine resolution imagery were available for describing the PMF. Joining the textural features and spectral features with the finer spatial resolution imagery for mapping PMF yields better results compared to using spectral or textural features alone. In addition, at higher resolution imagery, the contribution of the textural feature was greater than the spectral feature. The plastic mulch is 1 m in width, and separated by 0.2–0.5 m bare soil, and the objective of our study is to map the PMF at a paddock scale. Therefore, at the higher spatial resolution, the imagery obtains more detailed information with respect to the spectral feature, and increases the within-class differences. The textural features imagery is obtained by the statistics in a fixed moving window size, thus textural features can control the salt and pepper effect and highlight the spatial characteristic, and increase the inter-class differences. With the coarsening spatial resolution, the textural feature of PMF is lost, because the fixed moving window size to compute the textural feature corresponds to a larger field size and the patch size of PMF is mostly small and fragmented. Therefore, the contribution of the textural feature depends largely on the spatial resolution of the imagery rather than the spectral feature. As the spatial resolution becomes coarser, the contribution of the textural feature was decreased significantly.

(2) Spatial distribution of PMF obtained from different spatial resolution imagery

The spatial distribution of PMF in our study areas (Figures 7 and 8) was generated from a SVM with the aid of the developed three feature sets over the varying spatial resolution imagery.

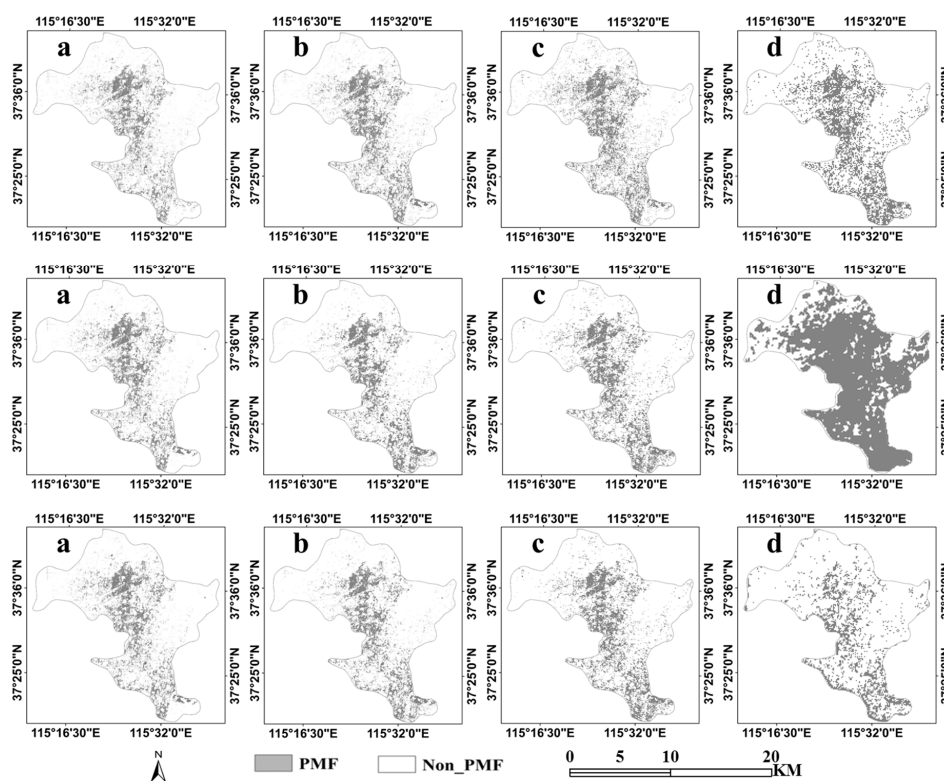


Figure 7. Spatial distribution of PMF in Jizhou (PMF extracted from Support Vector Machine (SVM) using spectral features, textural features and combined spectral and textural features from top to bottom, respectively at the spatial resolution of 6 m, 64 m, 100 m and 250 m from left to right).

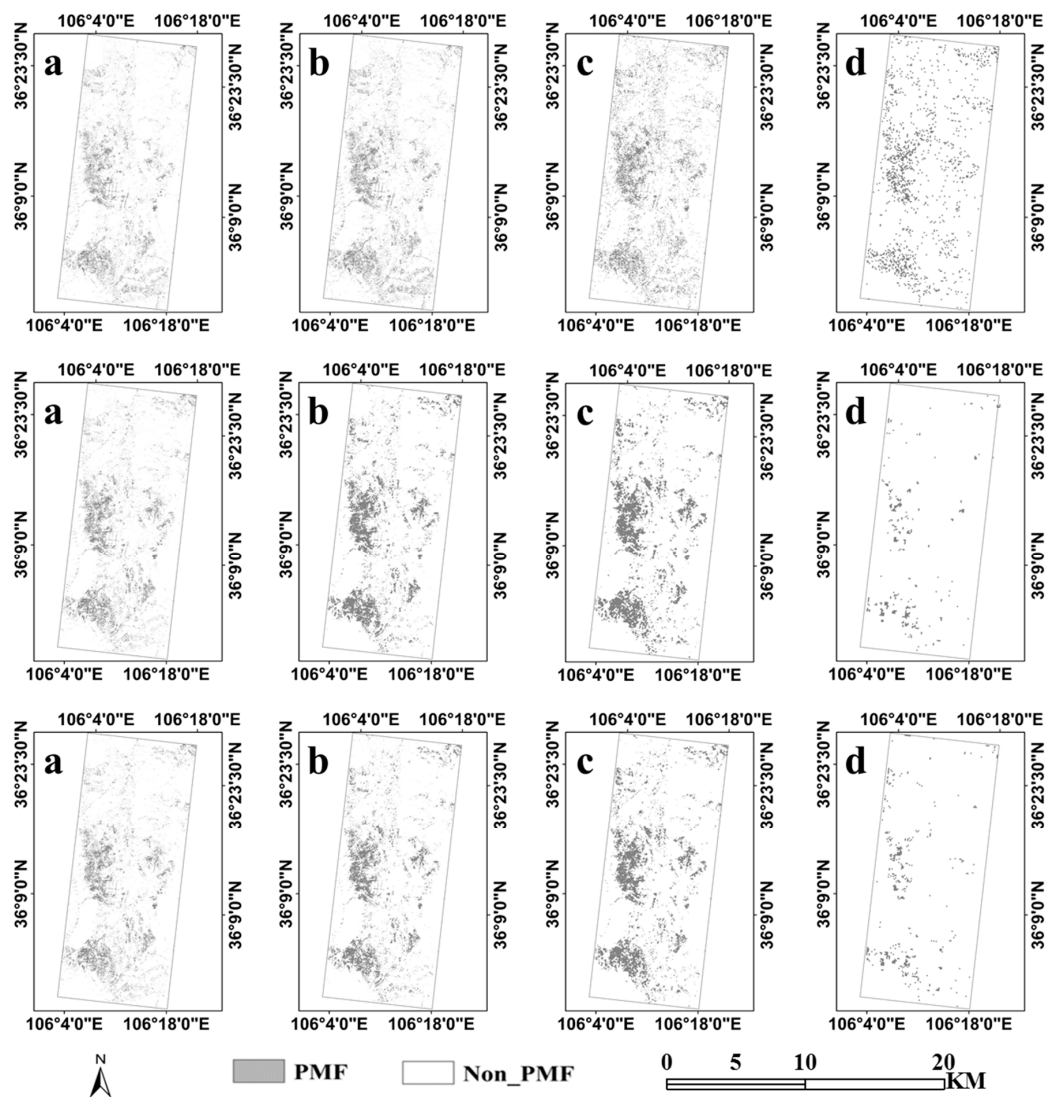


Figure 8. Spatial distribution of PMF in Guyuan (PMF extracted from a SVM using spectral features, textural features and combined spectral and textural features from top to bottom, respectively at the spatial resolution of 6 m, 64 m, 100 m and 250 m from left to right).

The spatial distributions of PMF in Jizhou extracted by SVM using different feature sets are displayed in Figure 7, taking PMF generated from different feature sets with spatial resolutions of 6 m, 64 m, 100 m and 250 m as examples. We can observe that most of the PMF in Jizhou was distributed in the central region and dispersed in the northern and southern regions. Marked differences were observed among the results generated from different feature sets across the varying spatial resolution. The distribution of PMF generated from the coarser spatial resolution imagery included more mismatching results than that from the finer resolution imagery. The spatial structure of PMF obtained from textural features from finer spatial resolution imagery was more obvious and reasonable than that from the spectral features. Over the varying spatial resolutions, the distribution of PMF from the coarser resolution imagery was extended further than that from the finer resolution imagery due to the greater commission error resulting from mixed pixels and blurred structural information. Such a phenomenon was similar across different feature sets but was more serious in the textural feature and less serious in the other two feature sets.

The spatial distributions of PMF in Guyuan extracted by SVM using different feature sets are displayed in Figure 8, taking PMF generated from the different feature sets with spatial resolutions of

6 m, 64 m, 100 m and 250 m as examples. We can observe that most of the PMF in Guyuan, Ningxia, were dispersed across whole regions. There are significant differences between feature sets over the varying spatial resolution. At the spatial resolution of 64 m and 100 m, the distribution area of PMF was larger than that from the finer resolution imagery due to the greater commission error resulting from mixed pixels and blurred structural information. Furthermore, at the spatial resolution of 250 m, the PMF is almost undetectable, particularly when using the textural or combined spectral and textural features.

4.2. Discussion

4.2.1. Relationship between Appropriate Spatial Scales from the ALV and the Spatial Resolution with the Highest Classification Accuracy from a SVM

In order to validate the effectiveness of the local variance method and to interpret the relationship between the appropriate spatial scales generated from the ALV and the spatial resolution with the highest classification accuracy, a SVM was used to extract the PMF in two study areas. Furthermore, we found that the appropriate spatial scales generated from the ALV were at a range of 8 m–20 m, and the highest classification accuracy from a SVM was at the spatial resolution of 6 m and 8 m in Jizhou and at the 6 m and 12 m in Guyuan (Table 4). Therefore, there is a proportional relation between the appropriate spatial scales generated from the ALV and the spatial resolution with the highest classification accuracy from a SVM: the spatial resolution with the highest classification accuracy is at the 1/2 location of the appropriate spatial scales generated from the ALV in Jizhou and at the 2/3 location of the appropriate spatial scales generated from the ALV in Guyuan. The reason is that the spatial pattern is similar in these two study areas during the selected time period, therefore, we got the same range of appropriate spatial scale by the ALV. However, the land cover/use types are different in these two areas, thus the spatial resolutions with the highest accuracy were different in these two study areas.

Table 4. Spatial resolution with the highest overall accuracy (OA), producer’s accuracy (PA) and user’s accuracy (UA) from different feature sets.

Spatial Resolution	Jizhou			Guyuan		
	OA	PA	UA	OA	PA	UA
Spectral Feature	10 m	8 m	8 m	6 m	6 m	6 m
Textural Feature	6 m	6 m	8 m	12 m	12 m	12 m
Spectral and textural Feature	6 m	6 m	6 m	12 m	12 m	12 m

The local variance algorithm has been applied, ultimately aimed at defining an optimal spatial scale for investigating different geographic entities, and all obtained very promising result. Of course, the results were different in different applications. Nijland, W. et al. [8] have done a study about optimizing the spatial resolution for quantitative mapping of natural vegetation using the average local variance function based on a HyMap image, and found an optimal pixel size of 55 m and 95 m for mapping the LAI (Leaf Area Index) and aboveground biomass. Furthermore, it is also reported that the optimal spatial resolution can be detected effectively using average local variance functions. The optimized spatial resolution can provide an improvement of 7% to 17% in mapping accuracy when compared to the original image spatial resolution. Coops, N. et al. [25] applied the local variance function to the simulated high spatial resolution imagery for predicting the spatial pattern of forest stands, and results indicate that it is theoretically possible to derive the spatial pattern of trees within a high spatial resolution forested scene provided that crown size is estimated a priori. Lottering, R. et al. [15] utilized the local variance function for optimizing the spatial resolution based on the vegetation index computed from a WorldView-2 pan-sharpened imagery for predicting levels of *Gonipterus scutellatus* defoliation. They found that the optimal spatial resolution for low, medium,

high and severe levels of defoliation were 2.5 m, 2.5 m, 3.5 m and 4.5 m respectively. Furthermore, they also presented that, based on the sampling theorem, an appropriate spatial resolution was established at one-half of the optimal spatial resolution for each level of defoliation. Therefore, an appropriate spatial resolution would be established at 1.25, 1.25, 1.75 and 2.25 m for low, medium, high and severe levels of defoliation, respectively. Results suggested that optimizing the spatial resolution of remotely sensed imagery essentially improves the prediction of vegetation defoliation. Our result is consistent with the above referenced works.

Therefore, the local variance method is an effective way to determine the appropriate spatial scale for mapping the object with remote sensing. The highest accuracy may be inconsistent when using different data and methods in different regions. From the classification accuracy variation, the accuracy is above 85% in Jizhou and above 80% in Guyaun at the spatial resolution from 2 m to 32 m, therefore, we can conclude that if the purpose of the mapping is not to achieve the highest accuracy, then the medium resolution remote sensing data can provide a reliable result for mapping the spatial pattern of PMF in North and Northwest China.

4.2.2. Reason for Accuracy Changes

In our study, decreased accuracies were observed with coarsening spatial resolutions as a general tendency across different feature sets. Slighter reduction occurred for the spectral feature compared to the textural feature. In general, the patch size, the shape and the distribution pattern of objects are the factors that influence the mapping accuracy across a changing spatial resolution scale. Large isodiametric or block-shaped objects will be more spatially resistant to changing resolutions than objects whose patches tend to be long and thin. In a small-patched and fragmented ecosystem, coarser resolution imagery may no longer contain some of the small-patched objects, and the accuracy will be lost. These two study areas are the core agricultural region in China, which is characterized by small-patched and fragmented farmland. The PMF in our study area is relatively small patched (10–20 m by 100–150 m), distributed in a rectangular shape and separated by bare soil (0.2–0.5 m) or crops with a very narrow width, and is interspersed in most regions (Figure 9). Therefore, at the higher spatial resolution, the imagery obtains more detailed information with respect to the spectral feature, and increases the within-class differences. The textural features imagery is obtained by the statistics in a fixed moving window size, thus textural features can control the salt and pepper effect, highlight the spatial characteristic, and increase the inter-class differences. With the coarsening spatial resolution, the textural feature of PMF is lost, because the fixed moving window size to compute the textural feature corresponds to a larger field size and the patch size of PMF is mostly small and fragmented. Therefore, the contribution of the textural feature depends largely on the spatial resolution of the imagery rather than the spectral feature. Thus, the classification accuracy changed very little across resolutions from 2 m to 30 m, and changed significantly across resolutions from 30–100 m or 100–250 m. In coarser resolution imagery, the farmland's spatial pattern is lost, and its spectral signal is confused with other objects. The increase in spectral purity and spatial border clarity may explain the observed higher accuracies from the finer resolution imagery.

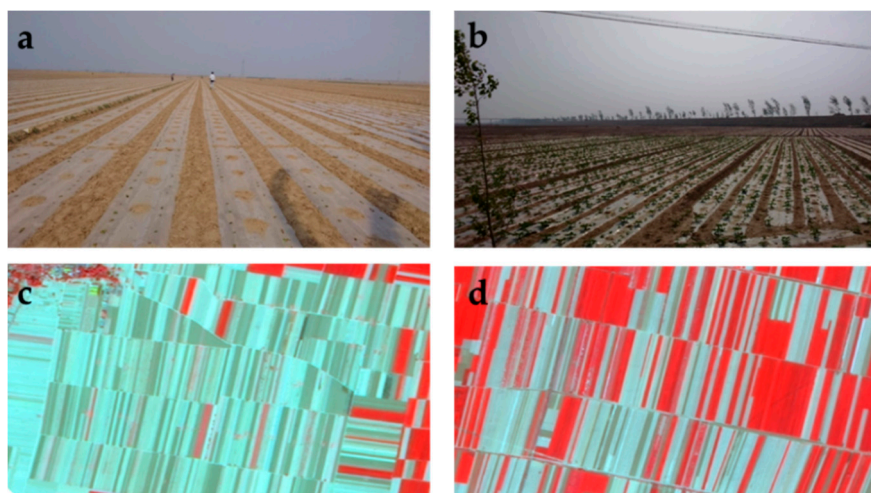


Figure 9. The PMF in Jizhou (a) Field photo of PMF at the sowing stage; (b) Field photo of PMF at the seedling stage; (c) PMF separated by bare soil in false colour composite (R: NIR, G: Red, B: Green) GF-1 imagery; (d) PMF separated by well-developed crops in false colour composite (R: NIR, G: Red, B: Green) GF-1 imagery.

4.2.3. Significance of Accuracy Changes

In order to explain and ensure the stability and the reliability of results, the confidence intervals of accuracies were estimated using the sample size, accuracy itself and the normal distribution (the sample size is large enough in our experiments). The confidence intervals for accuracies were calculated using a statistical approach that was previously presented [50]. A 99% confidence interval was used in our experiment.

For Jizhou, the confidence interval of the highest OA generated from spectral feature was between 89.87% and 94.15%; of textural features was between 93.88% and 98.03%; and of combined spectral and textural features was between 94.00% and 98.10%. Therefore, the OA of spectral based classification at the spatial resolutions from 2 m to 30 m was within the confidence interval of the highest OA; and the OA of the textural based classification and the combined spectral and textural based classification at the spatial resolutions from 2 m to 10 m was within the confidence interval of the highest OA of the textural based classification and the combined spectral and textural based classification respectively. Therefore, for the spectral based classification, the changes of obtained accuracies are not significant from 2 m to 30 m, above which they become more and more significant. While, for the textural or the combined spectral and textural based classification, the changes of obtained accuracies are not significant from 2 m to 10 m, above which they also become gradually significant.

For Guyuan, the confidence interval of the highest OA of the spectral based classification was between 80.49% and 87.66%; of textural features was between 85.59% and 92.08%; and of combined spectral and textural features was between 87.51% and 92.51%. Therefore, the accuracies of the spatial resolutions from 2 m to 26 m were within the confidence interval of the highest OA derived from the spectral based classification, and the spatial resolutions from 2 m to 20 m were within the confidence interval of the highest OA obtained from the textural based classification and the combined spectral and textural based classification. Therefore, for the spectral based classification, the changes of obtained accuracies are not significant from 2 m to 26 m, above which they become more and more significant. While, for the textural or the combined spectral and textural based classification, the changes of obtained accuracies are not significant from 2 m to 20 m, above which they also become progressively significant.

Therefore, for mapping the PMF in north or northwest China, the high to medium spatial resolution remote sensing data, such as the GF-1/2, HJ, or Landsat and so on, will provide a more acceptable result than coarse resolution data. However, there are no supported results and conclusion

about the performance of the higher resolution data, for example the sub-meter level (worldview-2), for mapping PMF.

The reason for the differences in the confidence intervals of accuracies between different features and the differences between the two study areas may be attributed to the land cover/use types, agricultural production mode and the used data. The land cover/use types in Guyuan are more complicated and fragmented than that in Jizhou, and the distribution pattern is more regular in Jizhou than Guyuan. Furthermore, the results also may be influenced by the temporal characteristic of the imagery and sensor specification. Because of the geographic position, climate types and the acquired time, the quality of the used data in Jizhou is better for classification than that in Guyuan.

4.2.4. The Influence of Textural Computing Parameters

In our study, the textural features from higher spatial resolution imagery provide powerful information for improving the mapping accuracy of PMF in our study area. However, in the GLCM texture extraction process, the computing window size, distance, orientation and quantization level are the important factors that contribute to the performance of textural-based classification [51,52]. Among them, the selection of the window size has a considerable influence on the textural-based classification results. Previous studies have also indicated that the optimal window size for extracting textural features is different for different land cover types. In theory, each land cover type should have a different appropriate computing scale for textural features, and at that scale, textural features may better play their role in imagery classification. Therefore, to discuss a relatively optimal window size for texture computing for mapping PMF and to express the influence of the window size, a set of window sizes was designed for extracting textures in the following section of our study. Based on a series of previous studies on textural-based classification, the window size length for extracting textural features was selected in the range from 3 pixels \times 3 pixels to 15 pixels \times 15 pixels (in odd order). Eight commonly used GLCM textural features were extracted from four bands, from the 8 m spatial resolution GF-1 satellite imagery from the small window size to the larger window size. We also used the SVM classifier to classify the above-mentioned five land cover types in Jizhou by textural features, to classify the combined spectral and textural features and to compare the classification accuracy (Table 5).

Table 5. Accuracy from textural features alone (combined spectral and textural features) across the different texture computing window sizes.

Window Size (Pixel)	OA	PA	UA	Kappa
3 \times 3	94.00 (94.33)	89.08 (88.82)	91.58 (93.17)	0.92 (0.93)
5 \times 5	94.70 (95.00)	88.45 (88.67)	93.21 (94.06)	0.93 (0.94)
7 \times 7	94.85 (95.23)	88.13 (88.86)	93.00 (93.91)	0.93 (0.94)
9 \times 9	94.98 (95.47)	88.31 (88.98)	92.72 (94.10)	0.94 (0.94)
11 \times 11	94.92 (95.69)	88.45 (89.55)	92.09 (93.97)	0.93 (0.94)
13 \times 13	94.69 (95.61)	88.06 (89.20)	91.52 (93.54)	0.93 (0.94)
15 \times 15	94.23 (95.44)	87.35 (88.62)	90.43 (93.35)	0.93 (0.94)

Table 5 shows that varied classification accuracies were observed over the different window sizes, although they were not very significantly different. As the window size increases, the OA and Kappa coefficient also tend to increase gradually and then decrease slightly when using both the textural features alone and the combined spectral and textural features. In addition, a similar tendency, but with fluctuations, was observed in PA and UA using the same feature sets. The window size with the peak value of the OA was larger than that of PA and UA using textural features alone, whereas such a window size was similar to that for the PA and UA using the combined spectral and textural features. When using the textural features alone, the OA reached the highest level of 94.98% with the 9 pixels \times 9 pixels window size, the PA achieved the best result of 89.08% with the 3 pixels \times 3 pixels

window size, and the UA reached the highest accuracy of 93.21% with the 5 pixels \times 5 pixels window size. When using the combined spectral and textural features, the OA reached the highest level of 95.69% with the 11 pixels \times 11 pixels window size, the PA achieved the best result of 88.98% with a window size of 9 pixels \times 9 pixels, and the UA obtained the highest accuracy of 94.10% with a window size of 9 pixels \times 9 pixels. Therefore, we can observe a rule that when using textural features alone for mapping the PMF, a smaller window size should be considered to extract textural features. On the other hand, when using both the spectral and textural features for mapping, a larger window size should be considered for extracting textural features. The selection of the window size for texture computing depends on the spatial resolution of the imagery and the spatial pattern of the interested objects [53]. Rodriguez-Galiano et al. suggested that a small window size provides a more representative description for a heterogeneous pattern, whereas larger window sizes may provide realistic representations of a homogeneous environment over large areas [54].

Simultaneously, we also examined the influence of the orientation in texture computing. We designed four computing orientations of 0°, 45°, 90° and 135° to extract the textural features using GF-1 imagery with 8 m spatial resolution. Furthermore, we found that the textural values were different among the different orientations, however, no significant impacts on the classification accuracy were observed.

4.2.5. The Contribution of Different Textural Types

A set of textural features having good discriminating ability is essential for a textural-based classification. The correlation between textural features and the redundancy information of a number of textural features may lead to poor classification results if we do not consider the separability of these features [55]. To further improve the classification accuracy and quality, the contribution of each textural feature for interclass separability should be fully analysed and expressed. An exhaustive evaluation of all textural features from multi-scale imagery is computationally prohibitive. Thus, we select a specific set of parameters, namely, 11 pixels \times 11 pixels window size, 45° orientation, distance of 1 pixel and a grayscale quantization level of 64, to explain the contributions of each of the eight commonly used GLCM textural features. Our experiments were conducted in two steps. In the first step, we combined the four spectral bands and the eight textural features individually from the blue/green/red/NIR (Near Infrared) bands, including 12 features, respectively. Then, we used the SVM to classify the land cover types and assess the mapping accuracy and selected the most effective band by comparing the mapping accuracy from different bands. According to the mapping accuracy of different bands (Table 6), it can be seen that there was not any significant difference in accuracy of the different bands. Therefore, in this second step, we selected the Near-Infrared band to examine the contribution of each textural feature. We combined the four spectral bands and each of the eight textural features from the Near-Infrared band to classify the land cover types and assess the accuracy (Table 7). From Table 6, we can find that the mean, dissimilarity and homogeneity were considered as more important textural features in our experiment for mapping PMF.

Table 6. The accuracy from combined spectral and textural features of different GF-1 bands.

Bands	OA	PA	UA	Kappa
Blue	95.40	89.86	94.09	0.94
Green	95.33	89.52	94.37	0.94
Red	95.63	92.05	87.23	0.94
Near Infrared	95.45	90.37	94.52	0.94

Table 7. The accuracy from combined spectral and each textural feature of the NIR bands.

Textures	OA	PA	UA	Kappa
Mean	92.34	90.45	93.28	0.90
Variance	91.29	88.09	89.66	0.89
Homogeneity	94.30	88.98	93.28	0.93
Contrast	92.26	88.55	90.45	0.90
Dissimilarity	94.16	89.01	93.46	0.92
Entropy	93.70	88.33	92.60	0.92
Angular Second moment	93.48	88.11	92.00	0.92
Correlation	91.19	88.03	88.42	0.89

As presented in the methods section, the mean reflects the regularity of texture, the dissimilarity is a measure of the changing degree of the gray level in imagery and the homogeneity represents the smoothness of the gray level distribution of imagery. On the one hand, the PMF in our study area is distributed in a rectangular shape in a large region of our study area, so PMF has the regularity texture. On the other hand, the PMF is separated by other non-plastic-mulched crops in a certain width in most cases, thus the changing degree of gray level carries a certain regularity. In addition, the thin smooth film surface will reduce the soil surface roughness to a certain degree, thus the homogeneity of PMF differs from the other land cover types. Therefore, the textural feature of the mean, dissimilarity and homogeneity make more contribution than others for mapping the PMF. As shown in Figure 10, the textural feature of PMF is significantly different from the other features.

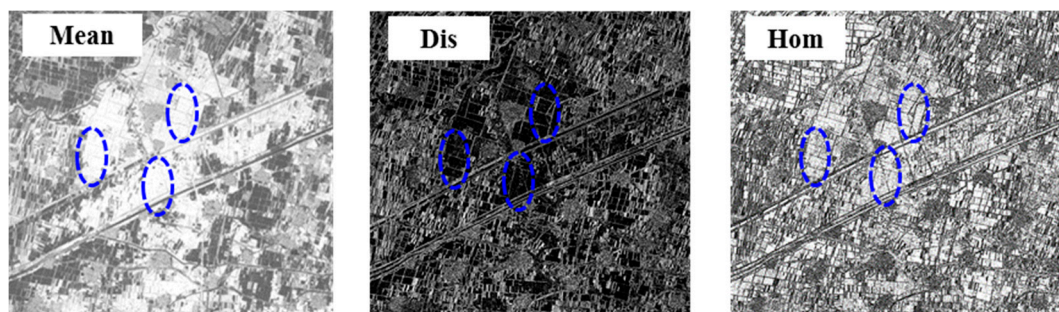


Figure 10. Example of different textural features extracted from the 8 m GF-1 imagery (In this figure, Dis is the abbreviation of dissimilarity and Hom is the abbreviation of homogeneity. Furthermore, the blue oval circled is PMF).

5. Conclusions

An appropriate spatial scale or a range of appropriate spatial scales is essential for mapping PMF with remote sensing, as all ground objects are better defined at specific spatial scales. This study used the ALV method to determine an appropriate spatial scale for mapping PMF using GF-1 imagery. Then, we sought to validate the effectiveness of the used method and to interpret the relationship between the appropriate spatial scale derived from the ALV and the spatial resolution with the highest accuracy; we classify the imagery with varying spatial resolution by means of SVM using the spectral features, textural features and the combined spectral and textural features respectively. Furthermore, we sought to evaluate the effects of spatial resolution on the classification ability of spectral and textural features for accurate mapping of PMF in Jizhou and Guyuan, China. The results from this study have illustrated that:

- (1) The 8 m–20 m spatial resolutions obtained from the ALV were selected as an effective range of appropriate spatial scale for mapping PMF both in Jizhou and Guyuan. However, there is a proportional relation: the spatial resolution with the highest classification accuracy is at the 1/2

location of the appropriate spatial scale generated from the ALV in Jizhou and at the 2/3 location in Guyuan.

- (2) By using the high spatial resolution GF-1 satellite imagery, we can successfully map the PMF in Northern China. The highest OA achieved 96.05% in Jizhou and 89.51% in Guyuan by jointly using the spectral and textural features.
- (3) The mapping accuracy of PMF decreased with the coarsening spatial resolution. However, there were differences between spectral and textural features. The accuracies generated from textural features varied more severely compared to that from spectral features with coarsening spatial resolution.
- (4) By analysing the significance of accuracy changes, we established that the accuracy changes are not significant at the spatial resolution of 2–30 m when using spectral features, and that they are not significant at the spatial resolution of 2–10 m and 2–20 m when using textural features and using combined spectral and textural features respectively. Therefore, if the mapping purpose is not to achieve the highest accuracy, then the high or medium resolution remote sensing data, such as GF-1/2, HJ, and Landsat imagery, can provide an acceptable result for mapping the spatial pattern of PMF in North and Northwest China.
- (5) The textural features perform better than spectral features at the higher spatial resolution. The textural features are slightly influenced by the computing parameters. Furthermore, among the textural features, the mean, the dissimilarity and the homogeneity make more contribution for mapping the PMF.

Overall, this study was the first attempt to determine an appropriate spatial scale for mapping PMF with remote sensing. The result is essential for understanding the importance of optimizing the spatial scale for better mapping of PMF and for the effective use of remote sensing data. Successfully mapping PMF with remote sensing depends largely on the selection of imagery at a suitable spatial scale. Furthermore, high spatial resolution satellite imagery should be more valuable for mapping PMF in small-patched and fragmented field regions. However, over large areas, the availability, cost and processing time may represent a limitation for mapping PMF.

Acknowledgments: This work was jointly supported by the National Natural Science Foundation of China (grant No. NSFC-61661136006), China Ministry of Agriculture “Introduction of International Advanced Agricultural Science and Technology Program (948 Program)” project (No. 2016-X38), and Open fund of Ministry of Agriculture Outstanding Researcher Fund and Key Laboratory of Agricultural Remote Sensing, Ministry of Agriculture, P.R. China (No. 2016003).

Author Contributions: Hasituya and Zhongxin Chen designed and conducted the experiments and contributed extensively in manuscript writing. Limin Wang and Jia Liu provided suggestions for the experiment design and the data analysis.

Conflicts of Interest: The authors declare no conflict of interest.

References

1. Yan, C.; Liu, E.; Shu, F.; Liu, Q.; Liu, S.; He, W. Review of agricultural plastic mulching and its residual pollution and prevention measures in China. *J. Agric. Res. Environ.* **2014**, *31*, 95–102.
2. Yan, C.R.; He, W.Q.; Liu, E.K.; Lin, T.; Pasquale, M.; Liu, S.; Liu, Q. Concept and estimation of crop safety period of plastic film mulching. *Trans. CSAE* **2015**, 1–4. [[CrossRef](#)]
3. Yan, C.; Mei, X.; He, W.; Zheng, S. Present situation of residue pollution of mulching plastic film and controlling measures. *Trans. CSAE* **2006**, *22*, 269–272.
4. Wang, H.H. Study on the Polarized Reflectance Characteristics of Agricultural Thin Membrane. Master’s Thesis, Northeast Normal University, Changchun, China, 2007.
5. Lu, L.Z.; Di, L.P.; Ye, Y. A Decision-Tree Classifier for Extracting Transparent Plastic-Mulched Landcover from Landsat-5 TM Images. *IEEE J.-STARS* **2014**, *7*, 4548–4558. [[CrossRef](#)]

6. Lu, L.Z.; Hang, D.; Di, L.P. Threshold model for detecting transparent plastic-mulched landcover using moderate-resolution imaging spectroradiometer time series data: a case study in southern Xinjiang, China. *J. Appl. Remote Sens.* **2015**, *9*. [[CrossRef](#)]
7. Hasituya; Chen, Z.X.; Wang, L.M.; Wu, W.B.; Jiang, Z.W.; Li, H. Monitoring Plastic-Mulched Farmland by Landsat-8 OLI Imagery Using Spectral and Textural Features. *Remote Sens.* **2016**, *8*, 353. [[CrossRef](#)]
8. Nijland, W.; Addink, E.A.; De Jong, S.M.; Van der Meer, F.D. Optimizing spatial image support for quantitative mapping of natural vegetation. *Remote Sens. Environ.* **2009**, *113*, 771–780. [[CrossRef](#)]
9. Schlerf, M.; Atzberger, C.; Hill, J. Remote sensing of forest biophysical variables using HyMap imaging spectrometer data. *Remote Sens. Environ.* **2005**, *95*, 177–194. [[CrossRef](#)]
10. Marceau, D.J.; Gratton, D.J.; Fournier, R.A.; Fortin, J.P. Remote sensing and the measurement of geographical entities in a forested environment. 2. The optimal spatial resolution. *Remote Sens. Environ.* **1994**, *49*, 105–117. [[CrossRef](#)]
11. Atkinson, P.M. Selecting the spatial resolution of airborne MSS imagery for small-scale agricultural mapping. *Int. J. Remote Sens.* **1997**, *18*, 1903–1917. [[CrossRef](#)]
12. Treitz, P.; Howarth, P. High spatial resolution remote sensing data for forest ecosystem classification: An examination of spatial scale. *Remote Sens. Environ.* **2000**, *72*, 268–289. [[CrossRef](#)]
13. Menges, C.H.; Hill, G.; Ahmad, W. Use of airborne video data for the characterization of tropical savannas in northern Australia: The optimal spatial resolution for remote sensing applications. *Int. J. Remote Sens.* **2001**, *22*, 727–740. [[CrossRef](#)]
14. Tran, T.D.; Puissant, A.; Badariotti, D.; Weber, C. Optimizing Spatial Resolution of Imagery for Urban Form Detection—The Cases of France and Vietnam. *Remote Sens.* **2011**, *3*, 2128–2147. [[CrossRef](#)]
15. Lottering, R.; Mutanga, O. Optimising the spatial resolution of WorldView-2 pan-sharpened imagery for predicting levels of *Gonipterus scutellatus* defoliation in KwaZulu-Natal, South Africa. *ISPRS J. Photogramm.* **2016**, *112*, 13–22. [[CrossRef](#)]
16. De Castro, A.I.; Ehsani, R.; Ploetz, R.; Crane, J.H.; Abdulridha, J. Optimum spectral and geometric parameters for early detection of laurel wilt disease in avocado. *Remote Sens. Environ.* **2015**, *171*, 33–44. [[CrossRef](#)]
17. Roth, K.L.; Roberts, D.A.; Dennison, P.E.; Peterson, S.H.; Alonzo, M. The impact of spatial resolution on the classification of plant species and functional types within imaging spectrometer data. *Remote Sens. Environ.* **2015**, *171*, 45–57. [[CrossRef](#)]
18. Shang, B. Quality Inspection and Quality Analysis of Hebei Province Jizhou City Environment. Master's Thesis, Northwest Agriculture & Forestry University, Shanxi, China, 2014.
19. Yuan, H.Y.; Zhang, X.Y.; Xu, H.J.; Yang, X.G. Changes of China agricultural climate resources under the background of climate change. V. Change characteristics of agricultural climate resources in Ningxia. *Chin. J. Appl. Ecol.* **2011**, *22*, 1247–1254.
20. Song, Y.Y.; Mi, W.B.; Bu, X.Y. Optimizing the spatial distribution of agricultural industry in Ningxia based on virtual water strategy. *Res. Agric. Modernization* **2015**, *36*, 92–98.
21. Guo, Y.J.; Mi, W.B.; Zhao, H.Y. Spatial variation and relevant influence factors of green development levels among the counties in Ningxia. *Econ. Geogr.* **2015**, *35*, 45–51.
22. Gao, H.; Gu, X.; Yu, T.; Liu, L.; Sun, Y.; Xie, Y.; Liu, Q. Validation of the calibration coefficient of the GaoFen-1 PMS sensor using the Landsat 8 OLI. *Remote Sens.* **2016**, *8*, 132. [[CrossRef](#)]
23. Woodcock, C.E.; Strahler, H.A. The Factor of Scale in Remote Sensing. *Remote Sens. Environ.* **1987**, *21*, 311–332. [[CrossRef](#)]
24. Hyppanen, H. Spatial autocorrelation and optimal spatial resolution of optical remote sensing data in boreal forest environment. *Int. J. Remote Sens.* **1996**, *17*, 3441–3452. [[CrossRef](#)]
25. Coops, N.; Culvenor, D. Utilizing local variance of simulated high spatial resolution imagery to predict spatial pattern of forest stands. *Remote Sens. Environ.* **2000**, *71*, 248–260. [[CrossRef](#)]
26. Song, C.; Woodcock, C.E. The spatial manifestation of forest succession in optical imagery the potential of multiresolution imagery. *Remote Sens. Environ.* **2002**, *82*, 271–284. [[CrossRef](#)]
27. Drăguț, L.; Eisank, C.; Strasser, T. Local variance for multi-scale analysis in geomorphometry. *Geomorphology* **2011**, *130*, 162–172. [[CrossRef](#)] [[PubMed](#)]
28. Ismail, R.; Mutanga, O.; Kumar, L.; Bob, U. Determining the optimal spatial resolution of remotely sensed data for the detection of *sirex noctilio* infestations in pine plantations in kwazulu-natal, south africa. *S. Afr. Geogr. J.* **2008**, *90*, 22–30. [[CrossRef](#)]

29. Marceau, D.J.; Howarth, P.J.; Gratton, D.J. Remote sensing and the measurement of geographical entities in a forested environment. 1. The scale and spatial aggregation problem. *Remote Sens. Environ.* **1994**, *49*, 93–104. [[CrossRef](#)]
30. Zheng, H. Study the Fundamentals of Detecting Spatial Pattern in Remote Sensing Images by Comparing Average Local Variance with Semi-Variograms. Ph.D. Thesis, University of Chinese Academy of Sciences, Beijing, China, 2014.
31. Bocher, P.K.; McCloy, K.R. The fundamentals of average local variance—part I: Detecting regular patterns. *IEEE Trans. Image Process.* **2006**, *15*, 300–310. [[CrossRef](#)] [[PubMed](#)]
32. Bocher, P.K.; McCloy, K.R. The fundamentals of average local variance—Part II: Sampling simple regular patterns with optical imagery. *IEEE Trans. Image Process.* **2006**, *15*, 311–318. [[CrossRef](#)] [[PubMed](#)]
33. Liu, J.X.; Liu, H.P.; Lv, Y.; Xue, X.J. Classification of high resolution imagery based on fusion of multiscale texture features. In Proceedings of the 35th International Symposium on Remote Sensing of Environment, Beijing, China, 22–26 April 2013. [[CrossRef](#)]
34. Coburn, C.A.; Roberts, A. A multiscale texture analysis procedure for improved forest stand classification. *Int. J. Remote Sens.* **2004**, *25*, 4287–4308. [[CrossRef](#)]
35. Angel Castillo-Santiago, M.; Ricker, M.; de Jong, B.H.J. Estimation of tropical forest structure from SPOT-5 satellite images. *Int. J. Remote Sens.* **2010**, *31*, 2767–2782. [[CrossRef](#)]
36. Pathak, V.; Dikshit, O. A new approach for finding an appropriate combination of texture parameters for classification. *Geocarto Int.* **2010**, *25*, 295–313. [[CrossRef](#)]
37. Estes, L.D.; Reillo, P.R.; Mwangi, A.G.; Okin, G.S.; Shugart, H.H. Remote sensing of structural complexity indices for habitat and species distribution modeling. *Remote Sens. Environ.* **2010**, *114*, 792–804. [[CrossRef](#)]
38. Kayitakire, F.; Hamel, C.; Defourny, P. Retrieving forest structure variables based on image texture analysis and IKONOS-2 imagery. *Remote Sens. Environ.* **2006**, *102*, 390–401. [[CrossRef](#)]
39. Ghosh, A.; Joshi, P.K. A comparison of selected classification algorithms for mapping bamboo patches in lower Gangetic plains using very high resolution WorldView 2 imagery. *Int. J. Appl. Earth Obs.* **2014**, *26*, 298–311. [[CrossRef](#)]
40. Fan, H. Land-Cover mapping in the Nujiang Grand Canyon: Integrating spectral, textural, and topographic data in a random forest classifier. *Int. J. Remote Sens.* **2013**, *34*, 7545–7567. [[CrossRef](#)]
41. Wang, T.; Zhang, H.; Lin, H.; Fang, C. Textural-Spectral feature-based species classification of mangroves in mai po nature reserve from Worldview-3 imagery. *Remote Sens.* **2016**, *8*, 24. [[CrossRef](#)]
42. Huang, X.; Liu, X.; Zhang, L. A Multichannel gray level co-occurrence matrix for multi/hyperspectral image texture representation. *Remote Sens.* **2014**, *6*, 8424–8445. [[CrossRef](#)]
43. Mountrakis, G.; Im, J.; Ogole, C. Support vector machines in remote sensing: A review. *ISPRS J. Photogramm.* **2011**, *66*, 247–259. [[CrossRef](#)]
44. Pal, M.; Mather, P.M. Support vector machines for classification in remote sensing. *Int. J. Remote Sens.* **2005**, *26*, 1007–1011. [[CrossRef](#)]
45. Melgani, F.; Bruzzone, L. Classification of hyperspectral remote sensing images with support vector machines. *IEEE Trans. Geosci. Remote Sens.* **2004**, *42*, 1778–1790. [[CrossRef](#)]
46. Heinzl, J.; Koch, B. Investigating multiple data sources for tree species classification in temperate forest and use for single tree delineation. *Int. J. Appl. Earth Obs.* **2012**, *18*, 101–110. [[CrossRef](#)]
47. Angelo, J.J.; Duncan, B.W.; Weishampel, J.F. Using lidar-derived vegetation profiles to predict time since fire in an oak scrub landscape in East-Central Florida. *Remote Sens.* **2010**, *2*, 514–525. [[CrossRef](#)]
48. Duro, D.C.; Franklin, S.E.; Dube, M.G. A comparison of pixel-based and object-based image analysis with selected machine learning algorithms for the classification of agricultural landscapes using SPOT-5 HRG imagery. *Remote Sens. Environ.* **2012**, *118*, 259–272. [[CrossRef](#)]
49. Vapnik, V.N. *The Nature of Statistical Learning Theory*; Springer: New York, NY, USA, 2000.
50. Keller, G. *Managerial Statistics*, 9th ed.; South Western Educational Publishing: Mason, OH, USA, 2011; p. 784.
51. Murray, H.; Lucieer, A.; Williams, R. Texture-Based classification of sub-Antarctic vegetation communities on Heard Island. *Int. J. Appl. Earth Obs.* **2010**, *12*, 138–149. [[CrossRef](#)]
52. Onojeghuo, A.O.; Blackburn, G.A. Mapping reedbed habitats using texture-based classification of QuickBird imagery. *Int. J. Remote Sens.* **2011**, *32*, 8121–8138. [[CrossRef](#)]

53. Gao, T.; Zhu, J.; Zheng, X.; Shang, G.; Huang, L.; Wu, S. Mapping spatial distribution of larch plantations from multi-seasonal Landsat-8 OLI imagery and multi-scale textures using random forests. *Remote Sens.* **2015**, *7*, 1702–1720. [[CrossRef](#)]
54. Rodriguez-Galiano, V.F.; Chica-Olmo, M.; Abarca-Hernandez, F.; Atkinson, P.M.; Jeganathan, C. Random Forest classification of Mediterranean land cover using multi-seasonal imagery and multi-seasonal texture. *Remote Sens. Environ.* **2012**, *121*, 93–107. [[CrossRef](#)]
55. Zhao, Y.; Zhang, L.; Li, P.; Huang, B. Classification of high spatial resolution imagery using improved gaussian markov random-field-based texture features. *IEEE Trans. Geosci. Remote Sens.* **2007**, *45*, 1458–1468. [[CrossRef](#)]



© 2017 by the authors. Licensee MDPI, Basel, Switzerland. This article is an open access article distributed under the terms and conditions of the Creative Commons Attribution (CC BY) license (<http://creativecommons.org/licenses/by/4.0/>).